

Inclusion of deuterated glycopeptides provides increased sequence coverage in hydrogen/deuterium exchange mass spectrometry analysis of SARS-CoV-2 spike glycoprotein

Christopher A. Haynes¹, Theodore R. Keppel¹, Betlehem Mekonnen¹, Sarah H. Osman¹, Yu Zhou¹, Adrian R. Woolfitt¹, Jakub Baudys¹, John R. Barr¹, and D Wang¹

¹Centers for Disease Control and Prevention

September 15, 2023

Abstract

Rationale. Hydrogen/deuterium exchange mass spectrometry (HDX-MS) can provide precise analysis of a protein’s conformational dynamics across varied states, such as heat-denatured vs. native protein structures, localizing regions that are specifically affected by such conditional changes. Maximizing protein sequence coverage provides high confidence that regions of interest were located by HDX-MS, but one challenge for complete sequence coverage is N-glycosylation sites. The deuteration of peptides post-translationally modified by asparagine-bound glycans (glycopeptides) has not always been identified in previous reports of HDX-MS analyses, causing significant sequence coverage gaps in heavily glycosylated proteins and uncertainty in structural dynamics in many regions throughout a glycoprotein. **Methods.** We detected deuterated glycopeptides with a Tribrid Orbitrap Eclipse mass spectrometer performing data-dependent acquisition. An MS scan was used to identify precursor ions, if high-energy collision-induced dissociation (HCD) MS/MS of the precursor indicated oxonium ions diagnostic for complex glycans then electron transfer low-energy collision-induced dissociation (EThcD) MS/MS scans of the precursor identified the modified asparagine residue and the glycan’s mass. As in traditional HDX-MS the identified glycopeptides were then analyzed at the MS level in samples labeled with D₂O. **Results.** We report HDX-MS analysis of the SARS-CoV-2 spike protein ectodomain in its trimeric pre-fusion form, which has 22 predicted N-glycosylation sites per monomer, with and without heat treatment. We identified glycopeptides and calculated their average isotopic mass shifts from deuteration. Inclusion of the deuterated glycopeptides increased sequence coverage of spike ectodomain from 76% to 84%, demonstrated that glycopeptides had been deuterated, and improved confidence in results localizing structural re-arrangements. **Conclusion.** Inclusion of deuterated glycopeptides improves the analysis of the conformational dynamics of glycoproteins such as viral surface antigens and cellular receptors.

INTRODUCTION

Spike is a trimeric surface glycoprotein from the SARS-CoV-2 virus causing the COVID-19 pandemic (1, 2). Spike’s binding to human angiotensin-converting enzyme 2 (ACE2) is critical for SARS-CoV-2 penetration of a host cell and initiation of infection (3, 4, 5). Spike is the surface antigen and target of all currently available COVID-19 vaccines (6), and improved understanding of spike’s structures and functions is likely to result in more effective SARS-CoV-2 vaccines (7).

Spike trimers engage in several dynamic structural changes related to binding ACE2, cleavage by protease TMPRSS2, unfolding their S2 domains, and finally re-folding to pull viral and target cell membranes into juxtaposition (8). Spike’s structural re-arrangements are required steps during SARS-CoV-2 infection (9) and are also potential mechanistic targets for spike-neutralizing reagents such as the host’s antibodies (10, 11). A well-established methodology to measure changes in (glyco)protein higher-order structure is hydrogen/deuterium exchange mass spectrometry (HDX-MS) (12). Previous publications have described HDX-MS

analyses of spike, including its interaction with ACE2 (4, 5, 13, 14) and changes in structural dynamics specific to different variants of concern, including Alpha, Beta, Delta, and Omicron (1, 13, 15, 16).

HDX-MS provides a framework of sample preparation, proteolytic digestion, peptide identification, and deuterium uptake measurement over time to identify changes in (glyco)protein conformation (12, 17). In an HDX-MS analysis comparing two states of the (glyco)protein of interest, changes in a peptide’s amide backbone hydrogen exchange are interpreted as indications of movement or stabilization of α -helices, β -sheets, and other hydrogen bonds contributing to secondary structure (18). Solvent accessibility also plays a role in the deuterium labeling of proteins (19).

An important goal of HDX-MS analysis is maximizing sequence coverage of the (glyco)protein of interest, since gaps could include regions with informative deuterium labeling. For example, localization of a monoclonal antibody’s epitope (20) on an antigenic (glyco)protein of interest can be challenging if sequence coverage of the antigenic (glyco)protein such as spike (16, 21) is incomplete (22). A key step in modern HDX-MS analysis for obtaining sequence coverage is on-line proteolytic digestion (23) of the (glyco)protein of interest to generate peptides amenable to liquid chromatography (LC)/MS detection. HDX-MS sample preparation typically includes a low pH (~2.5) quenching step immediately before proteolytic digestion (12), limiting digestion to acid-tolerant proteases such as pepsin (24) or aspergillopepsin (23, 25). These proteases generate overlapping, mostly non-specific (26) peptides that are nonetheless reproducible for a given protein substrate. Previous HDX-MS analyses of spike have shown sequence coverage gaps when using on-line digestion with pepsin (1, 4, 5, 13).

Specifically considering glycoproteins, sequence coverage gaps in HDX-MS analyses are often associated with N-glycosylation “sequons” (the amino acid sequence Asn-Xaa-Ser/Thr, where Xaa is not Pro and a glycan portion composed of 2 to 11+ hexose subunits is covalently bound to the Asn residue) (27). The reasons for these coverage gaps at N-glycosylation sequons potentially include 1) steric inhibition of the on-line protease’s cleavage by the bulky glycan group covalently bound to an Asn residue (28), resulting in fewer short peptides containing the sequon, and 2) lack of detection of the resulting high-mass glycopeptides during subsequent LC/MS and LC/tandem mass spectrometry (LC/MS/MS) analyses. Although several previous HDX-MS analyses of spike (4, 15) or IgG (29) have detected peptides containing the amino acid sequence Asn-Xaa-Ser/Thr, these are not *bona fide* “glycopeptides” because the mass(es) and possible identity(ies) of any covalently bound glycan group(s) were not specified. Some recent HDX-MS publications (1, 14) report glycopeptide data from a separate (non-HDX) analysis but this does not provide information about the deuteration of peptides with covalently bound glycans.

Glycan identity is an important aspect of glycoprotein analysis because microheterogeneity (the cohort of all the different glycan structures bound to a particular N-glycosylation sequon, (30)) influences glycoprotein structures and functions (31). The impact of microheterogeneity on HDX-MS analyses of glycoproteins is not presently known because detecting and identifying glycopeptides with their glycans still covalently bound requires advanced MS/MS methods and appropriate data processing for detection and assignment of glycans (32, 33, 34, 35).

SARS-CoV-2 Spike glycoprotein has 22 N-glycosylation sequons per monomer and several publications describe spike’s microheterogeneity (32, 36, 37, 38). Spike’s high level of glycosylation has caused significant gaps in sequence coverage and incomplete HDX-MS data in previous studies (1, 4, 5, 13). During our HDX-MS analyses of spike we applied a previously described method for detecting glycopeptides (39, 40) to the deuterium-labeled D614G variant (41). We believe this is the first report directly measuring the deuteration of peptides with N-glycosylation sequons and covalently bound glycan groups to determine the impact of microheterogeneity on the HDX-MS dynamics of SARS-CoV-2 spike. Heat-treatment of spike was used to significantly change protein structure and demonstrate the utility of deuterated glycopeptide data to improve HDX-MS conformational analysis of glycoproteins.

EXPERIMENTAL SECTION

Chemicals and Reagents.

Phosphate-buffered saline (PBS) tablets, LC/MS grade water 0.1% formic acid, methanol and acetonitrile 0.1% formic acid were from Fisher Scientific (PA). Deuterium oxide (99.9%) was from Cambridge Isotope Laboratories (MA). Urea and tris(carboxyethyl)phosphine (TCEP) were from Sigma-Aldrich (MO). Reagent and sample vials for HDX-MS were from Trajan Scientific and Medical (NC) and Thermo Scientific (CA), respectively.

Plasmid Design and Cell Culture.

The SARS-CoV-2 D614G spike protein ectodomain expression plasmid was designed as follows: amino acids 1-1208, furin cut site PRRAR substituted to PGSAS, 6 HexaPro stabilization substitutions (K986P, V987P, F817P, A892P, A899P, A924P), a T4 fold self-trimerization domain, and a polyhistidine tag for purification by nickel-charged nitrilotriacetic acid (Ni-NTA). FASTA sequences for 614G and Omicron spike constructs are in Supporting Information. Expi293F cells were obtained from ThermoFisher as part of the Expi293F protein expression system. Cells were cultured for 3+ passages at 37°C/125 RPM/8% CO₂ not exceeding a density of 5 × 10⁶ cells/ml or passage >30, seeded at a density of 2.5 × 10⁶ cells/mL one day prior to transfection, and diluted to 3 × 10⁶ cells/mL immediately before transfection. Plasmid was transfected at 1 µg DNA per 1 mL of cell culture using ExpiFectamine and Opti-Mem I Reduced Serum Medium (Thermo Scientific). Transfected culture was left to express for four days at 30°C/125 RPM/8% CO₂ before harvesting and centrifuging twice at 4°C/3000 RCF for 10 minutes to clarify the supernatant.

Protein Purification.

Three mL of 1 M imidazole (Sigma-Aldrich) per 100 mL of transfected clarified supernatant was added prior to purification. Purification used two buffers, one binding buffer (20 mM sodium phosphate, 500 mM sodium chloride, 30 mM imidazole pH 7.4) and one elution buffer (20 mM sodium phosphate, 500 mM sodium chloride, 500 mM imidazole pH 7.4). The column was first equilibrated with 5 column volumes (CV) of binding buffer. The supernatant was then loaded onto an AKTA Avant 150 FPLC through a Cytiva 5 mL HisTrap FF column at 0.5 mL/min. After sample loading, the column was washed with 5 CV binding buffer. The protein was eluted off the column using a gradient elution from 100% binding buffer to 100% elution buffer over 5 CV and peaks were collected in 2 mL fractions at 4°C. The peak fractions were loaded onto a 7K MWCO Zeba desalting column at 4°C, buffer exchanged into 300 mM sodium chloride, 20 mM Tris-HCl pH 8, and later concentrated on an Amicon 100K MWCO Ultra-15 centrifugal filter column at 4000 RCF at 4°C until desired concentration/volume was met. A minimum of 500 µg of this affinity purified protein was then loaded onto a Cytiva Superose 6 Increase 10/300 gel filtration column also on the AKTA Avant 150 system. Preparative size exclusion chromatography took place at 0.5 mL/min in 300 mM sodium chloride, 20 mM Tris-HCl pH 8. Peaks corresponding to the size of spike trimer were then fractionated into 2 mL fractions and later concentrated on a 100K MWCO Amicon filter if needed. Protein quality was checked by SDS-PAGE gel and analytical size exclusion chromatography before use.

Heat-treatment, Trypsin Digestion and Gel Analysis of Spike Ectodomain.

Spike ectodomain protein (Omicron variant, 1.3 µg/µL in 20 mM Tris, 300 mM NaCl, pH 8) was diluted 1:20 in HA buffer (100 mM Tris, 50 mM NaCl, pH 7.8) and 40 µL aliquots were incubated in a PCR tube and heater (Thermo Scientific) for 1 hour at 25, 35, 45, 55, and 65°C. After cooling to room temperature and centrifugation (1000 RPM, 10 min), supernatants were transferred to clean PCR tubes for trypsin digestion. Sequencing grade trypsin (Promega, WI) was diluted in HA buffer so that adding 2 µL of trypsin to each heat denatured aliquot resulted in a 1:100 molar ratio of trypsin to spike. A control set of aliquots had 2 µL of HA buffer with no trypsin added to verify heat-treatment did not result in aggregation. All tubes were incubated for 1 hour at 37°C, cooled to room temperature, measured for volume loss and compensated with HPLC-grade water. A nonreducing Bis-Tris 4-12% gradient gel (Thermo Scientific) was used to detect size-resolved spike proteins (Figure S1).

Hydrogen/Deuterium Exchange Mass Spectrometry.

A DHR-PAL system (Trajan) was used for sample preparation, with sample tray at 20°C, quench tray at 4°C,

valve chamber & pre-chiller at 4°C, and digestion chamber at 8°C. Purified spike ectodomain (0.4 µg/µL) was mixed 1:5 (v/v) with PBS prepared using H₂O (equilibration buffer, measured pH 7.22) or D₂O (labeling buffer, measured pH 7.56). Labeling times were 0, 60, 240, and 960 sec with 3 technical replicates at each time. Samples were quenched with an equal volume of 2 M urea 0.5 M TCEP pH 2.5 and held at 4°C for 2 min. An UltiMate3000 UPLC system (binary nano pump and loading pump, Thermo Scientific) was used for subsequent online sample handling. Automated valve switching passed the quenched sample over a 2.1 × 20 mm Nepenthesin-2 / Pepsin mixed digestion column (AffiPro, CZ) at 100 µL/min H₂O 0.1% HCOOH for 2 minutes, trapping the resulting peptides on a 2.1 × 5 mm Fully Porous C18 guard column (Phenomenex, CA), then de-salted peptides at 300 µL/min for 4 minutes. Peptides were eluted and resolved by a gradient from 13 to 65% mobile phase B (95:5:0.1 CH₃CN / H₂O / HCOOH over 23 min on a 1 × 100 mm Luna Omega 1.6 µm 100 Å C18 column (Phenomenex, CA). A Tribrid Eclipse Orbitrap (OT) mass spectrometer (Thermo Scientific) with HESI-2 electrospray ion source and high-flow needle was operated in positive ion mode to detect peptides for 31 minutes. In all samples precursor scans of resolution 120K (at m/z 200) in the range 375-2000 m/z were acquired. For each MS scan, the top-10 abundant precursor features were selected for data-dependent MS/MS scans, selecting for an intensity threshold of 30K counts, monoisotopic peptide precursors, charge states 2⁺ to 8⁺ with an isolation window of 1.2 m/z , and not repeating precursor ions more than twice within 15 sec. Precursors were fragmented with HCD at 28% normalized collision energy (NCE) and centroid scanned in the OT with standard automatic gain control (AGC) target, automatic injection time, scan range 120-2000 m/z , and resolution 30K. If at least one of three selected oxonium ions was detected (HexNAc 204.0867 m/z , HexNAc fragment 138.0545 m/z , or HexNAcHex 366.1396 m/z) with 15 ppm mass tolerance then EThcD OT-MS2 scans were acquired of that precursor ion. Supplemental HCD was at 20% NCE with profile scans from 150-2000 m/z at resolution 50K using custom AGC target (500%) and fill time (90 msec). At the end of the analytical gradient, solvent transitioned to 90% mobile phase B for 6 min, and halfway through that time the analytical and trapping columns were put into back-flow washing mode by automated valve switching. After re-equilibration of the analytical column at 13% mobile phase B the injection cycle ended at 45 min. As recommended (42), the entire batch of control and heat denatured samples (all time points and technical replicates) was randomized for HDX-MS acquisition to minimize batch effects on interpreted differences in protein state, labeling time, and replicates. To allow access to the HDX data of this study, the HDX data summary table (Table S2) and the HDX data table (Table S3) are included in the supporting information as per consensus guidelines (42).

Data Processing.

Protein Metrics Inc. (CA) Byos HDX 4.6-37 searched the 6 data files from equilibration buffer samples (0 sec labeling time, control and heat denatured, 3 technical replicates each) to identify (glyco)peptides using MS/MS spectra. The search database included spike and both proteases. Both HCD and EThcD tandem mass spectra contributed to peptide spectral matching. Putative (glyco)peptides were then searched for in data files from all samples at the MS level (and appropriate retention times) to identify both unlabeled and deuterated peptides and visualize their isotopic envelopes. Initial spike results (heat-treatment vs. control, 1271 peptides) were narrowed by 1) default software filters (MS2 score > 15, minimum alt_rank_score/primary_rank_score > 0.99, maximum precursor m/z error ± 40 ppm, maximum retention time deviation ± 5 min) leaving 1056 peptides, and 2) removing peptides with MS/MS score < 150 leaving 106 of 205 glycopeptides, removing peptides with more than ± 10% average, maximum, or minimum “deuteration” in 0 sec samples, and removing peptides causing standard deviations >10% at any labeled time-point, leaving 561 peptides. Additional manual curation involved adjustment of the extracted ion chromatogram (EIC) window used to integrate MS data and generate an isotopic envelope, optimizing the intensity and specificity of that envelope. Peptides with inadequate intensity EICs to estimate deuteration were discarded.

RESULTS

Traditional HDX-MS analysis of a glycoprotein’s conformational dynamics often leaves large information gaps because of challenges in analyzing the deuterium uptake of glycopeptides. During our traditional HDX-MS analysis of SARS-CoV-2 spike protein, we found significant gaps in sequence coverage and a lack of

information in many areas of interest. To fill these sequence coverage gaps, we incorporated signature ion-triggered EThcD into HDX-MS analysis (final spike (glyco)peptide coverage in Figure S2).

Identification of glycopeptides used Fourier-transform mass spectrometry (FTMS) scans to detect precursor ions, and those above an intensity threshold were selected for high-energy collision-induced dissociation (HCD) FTMS/MS scans. This relatively energetic fragmentation yields abundant b- and y-ions for spectral matching to peptide sequences, but can also produce oxonium ions (such as HexNAc 204.0867 m/z , HexNAc fragment 138.0545 m/z , and Hex(2)NAc 366.1396 m/z) diagnostic for the presence of complex glycosylation of the precursor peptide (33, 39, 43, 44). The presence of these signature oxonium ions triggered data-dependent electron transfer low-energy collision-induced dissociation (EThcD) FTMS/MS of a fresh precursor ion packet, yielding peptide fragments retaining 1 or more hexose groups or intact glycan, ideally confirming the glycosylation sequon's location (45).

Glycopeptide inclusion improves sequence coverage.

Addition of EThcD to facilitate the detection and identification of glycopeptides during HDX-MS significantly improved sequence coverage and conformational dynamic analysis of SARS-CoV-2 614G spike protein (Figure S2). Glycopeptides were confidently identified at 9 out of the 22 potential occupied N-glycosylation sequons per monomer in spike 614G variant (Table S1, 41% sequon coverage and 84% overall coverage) after manual data processing. At 8 N-glycosylation sequons with confident peptide coverage only glycopeptides were identified, with the exception, N1074, covered by one non-glycosylated peptide (Figure 1C). Therefore, without the inclusion of EThcD for glycopeptide detection and identification, the sequon coverage would have dropped to 1 (5%) and overall spike coverage to 76% (Figures 1 & S2). Additionally, because nine N1074 glycopeptides had HexNAc(2)Hex(5) and HexNAc(2)Hex(6) glycans (Figure 1), the detection of only the non-glycosylated peptide may not represent the true conformational dynamics at N1074.

On-line digestion with nepenthesin-2 and pepsin allows analysis of deuterated peptides in acidified conditions, but the non-specific nature of digestion, along with the need for rapid digestion and LC separation, brings concerns of lowered signal per peptide, especially when layered with potential glycan structural diversity at each sequon. Despite these potential issues with sensitivity, N-glycosylation sequon-specific combinations of peptide and glycan diversity were observed (Figure 1). Seven glycopeptides (one in 2⁺ and 3⁺ charge states) with unique amino acid sequences including N234 displayed only one glycan type HexNAc(2)Hex(9). In contrast, 13 unique glycopeptide amino acid sequences including N603 displayed five or more glycan types, while the only glycopeptide amino acid sequence including N1134 displayed ten glycan types. Table S1 summarizes N-glycosylation sequon coverage and occupancy. All glycan groups at the 9 sequons with coverage were of similar types (oligomannose, complex, and hybrid) as described in previous publications on spike microheterogeneity (34, 39, 46).

Evidence for deuterated glycopeptides is shown in Figures 2 to 4 using glycopeptide 597-607 HexNAc(2)Hex(5) as an example. We obtained high-confidence (Byonic score = 508.5) MS/MS identification (Figure 2), reproducible extracted ion chromatograms (Figure 3A), and high-quality isotopic envelopes (Figure 3B). We observed that each unique amino acid sequence for a glycopeptide showed consistent uptake plots in both control and heat denatured states although they had different N-glycan groups. For example, glycopeptides with sequence ⁵⁹⁷VITPGTN TSNQ⁶⁰⁷ had highly consistent deuterium uptake (Figure 4, left peptide) even though 5 different glycan groups were identified on N603. However, overlay of composite uptake plots for all twelve N603 overlapping glycopeptides (Figure 4) indicated that unique amino acid sequences had different uptakes, and increasing glycopeptide length affected estimated deuteration. For example, C-terminally extending the above 597-607 glycopeptide by 2 amino acids decreased uptake in the control state but increased uptake after heat-treatment (Figure 4, center peptide). Our interpretation was that glycopeptide amino acid sequence at sequon N603 was a stronger determinant of deuteration than N-glycan identity.

Supporting this interpretation, glycopeptides covering sequons N61 and N234 showed two levels of deuteration in the heat denatured state on composite uptake plots, also associated with the length of glycopeptides. For

example, the N61 sequon’s proximity to the sequence⁶⁶HAIH⁶⁹ indicated that inclusion of this histidine-rich “cool” spot of deuteration decreased the percentage labeling of 7 longer glycopeptides ~15% after heat treatment compared to 4 overlapping but shorter glycopeptides that did not include the ⁶⁶HAIH⁶⁹sequence (Figure S3). This result is consistent with the slow deuteration of His residues (47, 48), and amino acid sequence being a stronger determinant of deuteration than N-glycan identity.

Isotopologue ratios of deuterated glycopeptide fragment ions.

Glycopeptide deuteration (Figures 2 to 4) and the presence of an amide bond in N-acetyl-hexosamines suggested that total glycopeptide deuteration included the N-acetyl amide group(s) of N-linked glycans, which has been previously confirmed at the glycan and glycopeptide levels (49) and recently reviewed (50). To measure N-acetyl hexose labeling, isotopologue ratios of glycopeptide⁵⁹⁷VITPGTN TSNQ⁶⁰⁷HexNAc(2)Hex(5) fragment ions were compared for both control and heat denatured states at all deuteration times. All MS/MS scans consistent with this glycopeptide precursor’s m/z and LC retention time were converted to lists of product ion m/z vs. intensity, and a ratio was taken between a fragment’s monoisotopic m/z (M0) and its M + 1 isotope’s m/z (M1, Figure 5 *inset*). The bottom-up peptide detection strategy of the Tribrid Orbitrap Eclipse (see Experimental Section) limited the number of MS/MS scans of each deuterated glycopeptide to 3 to 6 per data file.

First, the theoretical M0/M1 ratio for the HexNAc product ion ($[C_8H_{14}NO_5]^+$, M0 204.0867 m/z) is 11.5, similar to the observed 9.6 ± 2.9 ratio (Figure 5, C0 and H0, white bars). Second, the theoretical M0/M1 ratio for the \sim y8 product ion ($[C_{31}H_{52}N_{11}O_{15}]^+$, fragment ⁶⁰⁰PGTN TSNQ⁶⁰⁷ without the glycan attached, Figure 1) is 2.99, similar to the observed 2.24 ± 1.21 ratio (Figure 5, C0 and H0, grey bars). This establishes that the product ion isotopologue analysis is appropriate, despite a limited number of MS/MS scans as described above. Third, the \sim y8 product ion’s M0/M1 ratio significantly decreased after D₂O exposure (Figure 5, grey bars), consistent with deuteration of this peptide’s 7 amide groups, reducing the amount of M0 818.3639 m/z and increasing the amount of M1 819.3779 m/z . Fourth, the HexNAc product ion’s M0/M1 ratio also decreased after D₂O exposure (Figure 5, white bars), indicating that it was labeled with deuterium. Student’s T-test of the HexNAc product ion’s M0/M1 ratios at 0 and 960 seconds of D₂O exposure indicated a significant difference ($p = 0.002$), and these results collectively support deuteration at the amide proton in the N-acetyl moieties on glycans N-linked to glycopeptides. Corroborative data including two y-series product ions and HexNAc product ion for a different glycopeptide, 1132-1145 HexNAc(4)Hex(3)Fuc(1) is shown in Figure S4. An alternative explanation of this isotopologue analysis is the previously reported scrambling of deuterons between product ions during HCD (51, 52), and a different MS/MS strategy ((53, 54), beyond the scope of this study) would be needed to address that alternative, possibly including deconvolution of isotopic envelopes for product ions with 0, 1 and 2 deuterons.

Control state: no heat-treatment.

The workflow to include glycopeptides in HDX-MS analysis was then tested after inducing a substantial change in spike structure by comparing native and heat treated glycoprotein. Without heat treatment, spike ectodomain (glyco)peptides showed a range of D₂O labeling (interpreted as structural dynamics) between ~0% and ~37% that visually correlated with sub-domain location (Figure 6A). Localization of these patterns on a model based upon Protein Data Bank (PDB) files 6VSB and 6VXX (55) included key domains (furin cleavage site, fusion peptide, 630 loop, etc.) often missing from RCSB structures (www.rcsb.org), possibly because disordered regions of spike can have low electron density in cryo-EM analysis (56). The least deuterated area (<5%) was the trimeric core interface (764-782 helix, 997-1020 helix, and 1043-1062 strand in β -sheet), as previously described (4, 13).

The most deuterated regions (37%) were the “hinge” between head and stalk regions (1132-1145), furin cleavage site (672-690), and 630 loop (624-636), the latter also consistent with a previous report (13). Labeling of spike’s “hinge” is a novel HDX-MS result, completely based on the coverage of deuterated glycopeptides containing glycan-modified N1134 (Figures 6 and S2). Robust labeling (24-30%) was observed in the fusion peptide (823-851), N-terminus (19-31), and middle helix of the stalk (1174-1197).

The receptor binding domain (RBD) had the highest deuteration (27%) on a strand forming its hinge with the rest of S1 (319-346, including deuterated glycopeptide coverage at N343) and the two loops of the receptor binding motif (RBM, 442-452 and 471-487) for ACE2 (57). The other strand forming the RBD's hinge with S1 (516-533) was 20% deuterated. A central helix (784-795), a turn-helix-turn (939-977) and a helix U-turn (753-759) were also moderately deuterated (28-30%). The N-terminal domain (NTD) showed an outer segment (171-176) with moderate labeling (27%).

Several recent reports describe bimodality in isotopic envelopes for certain regions of spike (1, 13, 15); the only apparently bimodal peptide 878-904 in this study was interpreted to be chromatographic co-elution of two precursor peptides with the same charge state and overlapping precursor isotopic envelopes based on observing “bimodality” even at 0 sec (data not shown).

State difference (heat-treatment minus control).

Visualization of (heat – control) deuteration (Figure 6B), showed both increased and decreased labeling in different sub-domains of spike. Regions with no significant deuteration difference (within the ± 0.9 Da error of labeling estimation based upon average peptide length and repeatability, Table S2) were not interpreted to have “zero dynamic change” (42). Deuterated glycopeptide data provided coverage essential for revealing increased labeling with longer D₂O exposure times around sequons N61 (11-15%) and N234 (11-15%) in the NTD, N343 in the RBD (10-15%), N603 (14-19%) and N801 (9%) in the S2 domain, as well as N1074 (10-16%) and N1134 (13-6%) in the stalk. Interestingly, only N1134 glycopeptides in the stalk region showed diminishing differences from the control state with increasing D₂O exposure.

The region with lowest deuteration in the control state (trimer core interface) showed substantial increases in deuteration (764-782 helix, 21%, 1007-1024 helix, 20%, 1050-1062 β -strand, 20%). Regions with the highest deuteration in the control state showed only small increases [the “hinge” between head and stalk (1132-1145, 6%), the 630 loop (624-635, 5%)] or even reductions [the furin site (672-703, -8%) and fusion peptide (823-851, -2%)]. Data for changes in the “hinge” region were entirely from deuterated glycopeptides.

Increases in the deuteration of the RBD were interpreted as loosening of its sub-domain architecture, including outer loop 336-350 (10-24%) and the inner β -strand 393-399 (27%). In addition, the “hinge” of the RBD to S1 (515-533) and a loop of its RBM (442-453) had lower deuteration (-4%) after heat treatment. Furthermore, S2 domain helices interpreted to be dynamic and primed for fusion based on their substantial deuteration in the control state were lower (939-945 and 967-977, -5%) after heat treatment. Finally, the NTD showed spike's highest reduction in deuteration (-10%) after heat-treatment at its outermost tip (243-262). All these results are consistent with increased accessibility to limited trypsin digestion (Figure S1), looser inter-monomer interaction, and disruption of tight packing between 3 NTDs and 3 RBDs from heat treatment. Reductions in deuteration observed for the most labeled sub-domains in the control state (furin site as an example) were interpreted as spike glycoprotein shriveling or collapsing after heat treatment.

DISCUSSION

Comparing native and heat denatured SARS-CoV-2 spike demonstrated the utility of including deuterated glycopeptides in HDX-MS analyses of glycoprotein conformational dynamics. We conclude that 1) inclusion of 106 glycopeptides and 9 N-glycosylation sequons increased spike sequence coverage from 76% to 84%, 2) glycopeptides become deuterated and provide useful regional and protein-level information, 3) observed glycan identities are consistent with publications from non-deuterating studies (34, 39, 46), and 4) labeling of the amide nitrogens on N-acetyl groups of glycans merits inclusion in estimates of glycopeptide maximum deuteration.

Three sub-domains of spike glycoprotein which are known to have key functions during host cell infection by SARS-CoV-2 virus were adjacent to N-glycosylation sequons with confident deuterated glycopeptide coverage, including the 630 loop (N603), the S2' cleavage site that releases the fusion peptide (N801), and the fusion peptide itself (N801). By detecting up to 37% deuteration in the control state in these portions of spike we corroborate existing HDX-MS descriptions of spike dynamics (1, 14). However, by

adding information based on deuterated glycopeptides (N1134) we detected “hinge” motion between spike’s globular head and stalk, in addition to improved deuterated peptide resolution in the 630 loop, S2’ cleavage site, and fusion peptide. Using heat treatment to significantly change spike structure confirmed the utility of deuterated glycopeptide data by inducing a broader change in dynamics than a traditional HDX-MS state comparison such as binding to ACE2 (4, 14) or a monoclonal antibody (11, 21) would have induced. Pairing glycopeptide detection on a Tribrid Orbitrap Eclipse instrument with appropriate data analysis reveals dynamics of key spike sub-domains in proximity to N-glycosylation sequons, which has not been previously included in HDX-MS analyses (1, 4, 5, 13).

The identities of glycan groups that we detected at each N-glycosylation sequon were consistent with previous reports (33, 34, 39, 46), specifically with the most abundant glycans at each sequon. However, the microheterogeneity, or variety of glycan structures observed at each N-glycosylation sequon, for deuterated spike glycopeptides in this report did not indicate as many different glycan structures at each sequon as previously reported by others (39, 46), but this is not surprising given the differences in LC and MS/MS conditions in typical HDX-MS versus bottom-up glycopeptidomics analyses. For example, HDX-MS LC is typically conducted at relatively high flow rates (40 μ L/min or higher, (58)) with large-bore chromatography columns (1.0 or 2.1 mm) and steep gradients (10 to 20 minutes) to minimize deuterium back-exchange (59). All these LC conditions are non-ideal for sensitive glycopeptide detection, which performs best at nano-flow rates (< 1 μ L/min) with nano-electrospray ion sources and columns, and long gradients (1 to 2 hours). Given these limitations of HDX-MS LC, there is likely to be considerable room for improvement in the ionization, detection, and analysis of deuterated glycopeptides.

Analysis of product ions from deuterated glycopeptides supported previous reports (49, 50) of deuteration of N-acetyl hexose subunits of glycans attached to glycopeptides during HDX-MS analyses. The possibility of deuterium scrambling during HCD (51, 52) as the source of deuterated N-acetyl product ions cannot be excluded by our MS/MS data acquisition strategy, and a more targeted approach with ETD (53) or ultraviolet photo dissociation (UVPD) (54) MS/MS would be required. Deuteration of N-acetyl hexoses is significant because calculation of “maximum peptide deuteration” is based on the number of amino acid backbone amides that could have been labeled (all except the N-terminal 1 or 2 residues and any proline residues (60, 61)), so the presence of each N-acetyl group in a glycan structure could add one potential labeling site per glycopeptide. We are not aware of any HDX-MS data processing software that includes options for the deuteration of glycans attached to glycopeptides. Additional complexity is added by microheterogeneity, because glycans that differ in the number of N-acetyl groups will have different numbers of potential labeling sites. We will continue to explore the effect of glycan subunit composition on the maximum peptide deuteration level for different types of glycopeptides.

Inclusion of deuterated glycopeptides in HDX-MS is a step forward in attempts to measure glycoprotein dynamics under conditions that are as native as possible. Direct detection of deuterated glycopeptides from glycoproteins such as viral surface antigens and cellular receptors avoids additional HDX-MS procedures, for example de-glycosylation with PNGase before or after deuteration using acid-tolerant isoforms Rc (62), or H (63, 64). De-glycosylation adds time and complexity to sample preparation and potentially introduces additional back-exchange and/or artifacts during HDX-MS analyses. In the case of SARS-CoV-2 spike, previous reports indicate that glycans participate in modulation of the RBD moving to “up” or “down” positions (65), as well as in ACE2 interaction (66, 67), indicating the importance of measuring spike glycopeptide dynamics in a native state using HDX-MS.

Author Contributions

D.W., T.K. and C.H. conceptualized the study. S.O. prepared spike protein and B.M. performed heat-treatment. C.H. and T.K. performed HDX-MS. C.H. wrote the manuscript and all authors contributed to its review and editing.

Notes The authors declare no competing financial interest. The findings and conclusions in this report are

those of the authors and do not necessarily represent the official position of the Centers for Disease Control and Prevention. Use of trade names and commercial sources in this presentation is for identification only and does not imply endorsement by the Division of Laboratory Sciences, National Center for Environmental Health, Centers for Disease Control and Prevention, the Public Health Service, or the U.S. Department of Health and Human Services.

ACKNOWLEDGMENT

We thank Dr. Bin Zhou for the plasmids expressing the spike constructs used in this work.

REFERENCES

1. Braet SM, Buckley TSC, Venkatakrishnan V, Dam KA, Bjorkman PJ, Anand GS. Timeline of changes in spike conformational dynamics in emergent SARS-CoV-2 variants reveal progressive stabilization of trimer stalk with altered NTD dynamics. *Elife*. 2023;12.
2. Mehra R, Kepp KP. Structure and Mutations of SARS-CoV-2 Spike Protein: A Focused Overview. *ACS Infect Dis*. 2022;8(1):29-58.
3. Alabsi S, Dhole A, Hozayen S, Chapman SA. Angiotensin-Converting Enzyme 2 Expression and Severity of SARS-CoV-2 Infection. *Microorganisms*. 2023;11(3).
4. Raghuvamsi PV, Tulsian NK, Samsudin F, Qian X, Purushotorman K, Yue G, et al. SARS-CoV-2 S protein:ACE2 interaction reveals novel allosteric targets. *Elife*. 2021;10.
5. Narang D, James DA, Balmer MT, Wilson DJ. Protein Footprinting, Conformational Dynamics, and Core Interface-Adjacent Neutralization "Hotspots" in the SARS-CoV-2 Spike Protein Receptor Binding Domain/Human ACE2 Interaction. *J Am Soc Mass Spectrom*. 2021;32(7):1593-600.
6. Federico M. How Do Anti-SARS-CoV-2 mRNA Vaccines Protect from Severe Disease? *Int J Mol Sci*. 2022;23(18).
7. Corbett KS, Edwards DK, Leist SR, Abiona OM, Boyoglu-Barnum S, Gillespie RA, et al. SARS-CoV-2 mRNA vaccine design enabled by prototype pathogen preparedness. *Nature*. 2020;586(7830):567-71.
8. Jackson CB, Farzan M, Chen B, Choe H. Mechanisms of SARS-CoV-2 entry into cells. *Nat Rev Mol Cell Biol*. 2022;23(1):3-20.
9. Xia S, Liu M, Wang C, Xu W, Lan Q, Feng S, et al. Inhibition of SARS-CoV-2 (previously 2019-nCoV) infection by a highly potent pan-coronavirus fusion inhibitor targeting its spike protein that harbors a high capacity to mediate membrane fusion. *Cell Res*. 2020;30(4):343-55.
10. Zhao MM, Zhu Y, Zhang L, Zhong G, Tai L, Liu S, et al. Novel cleavage sites identified in SARS-CoV-2 spike protein reveal mechanism for cathepsin L-facilitated viral infection and treatment strategies. *Cell Discov*. 2022;8(1):53.
11. Silva RP, Huang Y, Nguyen AW, Hsieh CL, Olaluwoye OS, Kaoud TS, et al. Identification of a conserved S2 epitope present on spike proteins from all highly pathogenic coronaviruses. *Elife*. 2023;12.
12. Vinciauskaite V, Masson GR. Fundamentals of HDX-MS. *Essays Biochem*. 2023;67(2):301-14.
13. Calvaresi V, Wrobel AG, Toporowska J, Hammerschmid D, Doores KJ, Bradshaw RT, et al. Structural dynamics in the evolution of SARS-CoV-2 spike glycoprotein. *Nat Commun*. 2023;14(1):1421.
14. Chen C, Zhu R, Hodge EA, Diaz-Salinas MA, Nguyen A, Munro JB, et al. hACE2-Induced Allosteric Activation in SARS-CoV versus SARS-CoV-2 Spike Assemblies Revealed by Structural Dynamics. *ACS Infect Dis*. 2023;9(6):1180-9.
15. Costello SM, Shoemaker SR, Hobbs HT, Nguyen AW, Hsieh CL, Maynard JA, et al. The SARS-CoV-2 spike reversibly samples an open-trimer conformation exposing novel epitopes. *Nat Struct Mol Biol*.

2022;29(3):229-38.

16. Hanke L, Sheward DJ, Pankow A, Vidakovics LP, Karl V, Kim C, et al. Multivariate mining of an alpaca immune repertoire identifies potent cross-neutralizing SARS-CoV-2 nanobodies. *Sci Adv.* 2022;8(12):eabm0220.

17. Benhaim M, Lee KK, Guttman M. Tracking Higher Order Protein Structure by Hydrogen-Deuterium Exchange Mass Spectrometry. *Protein Pept Lett.* 2019;26(1):16-26.

18. Oganesyan I, Lento C, Wilson DJ. Contemporary hydrogen deuterium exchange mass spectrometry. *Methods.* 2018;144:27-42.

19. Liu XR, Zhang MM, Gross ML. Mass Spectrometry-Based Protein Footprinting for Higher-Order Structure Analysis: Fundamentals and Applications. *Chem Rev.* 2020;120(10):4355-454.

20. Haque HME, Mantis NJ, Weis DD. High-Throughput Epitope Mapping by Hydrogen Exchange-Mass Spectrometry. *J Am Soc Mass Spectrom.* 2023;34(1):123-7.

21. Seow J, Khan H, Rosa A, Calvaresi V, Graham C, Pickering S, et al. A neutralizing epitope on the SD1 domain of SARS-CoV-2 spike targeted following infection and vaccination. *Cell Rep.* 2022;40(8):111276.

22. Zhu S, Liuni P, Chen T, Houy C, Wilson DJ, James DA. Epitope screening using Hydrogen/Deuterium Exchange Mass Spectrometry (HDX-MS): An accelerated workflow for evaluation of lead monoclonal antibodies. *Biotechnol J.* 2022;17(2):e2100358.

23. Hamuro Y, Zhang T. High-Resolution HDX-MS of Cytochrome c Using Pepsin/Fungal Protease Type XIII Mixed Bed Column. *J Am Soc Mass Spectrom.* 2019;30(2):227-34.

24. Vorauer C, Wrigley MS, Rincon Pabon JP, Watson MJ, Mundorff CC, Weis DD, et al. Rapid Assessment of Pepsin Column Activity for Reliable HDX-MS Studies. *J Am Soc Mass Spectrom.* 2021;32(9):2386-90.

25. Mullahoo J, Zhang T, Clauser K, Carr SA, Jaffe JD, Papanastasiou M. Dual protease type XIII/pepsin digestion offers superior resolution and overlap for the analysis of histone tails by HX-MS. *Methods.* 2020;184:135-40.

26. Hamuro Y, Coales SJ. Optimization of Feasibility Stage for Hydrogen/Deuterium Exchange Mass Spectrometry. *J Am Soc Mass Spectrom.* 2018;29(3):623-9.

27. Chau TH, Chernykh A, Kawahara R, Thaysen-Andersen M. Critical considerations in N-glycoproteomics. *Curr Opin Chem Biol.* 2023;73:102272.

28. Xia Y, Ma Z, Qiu M, Guo B, Zhang Q, Jiang H, et al. N-glycosylation shields *Phytophthora sojae* apoplastic effector PsXEG1 from a specific host aspartic protease. *Proc Natl Acad Sci U S A.* 2020;117(44):27685-93.

29. Houde D, Arndt J, Domeier W, Berkowitz S, Engen JR. Characterization of IgG1 Conformation and Conformational Dynamics by Hydrogen/Deuterium Exchange Mass Spectrometry. *Anal Chem.* 2009;81(14):5966.

30. Zhang S, Li W, Lu H, Liu Y. Quantification of N-glycosylation site occupancy status based on labeling/label-free strategies with LC-MS/MS. *Talanta.* 2017;170:509-13.

31. Wu D, Struwe WB, Harvey DJ, Ferguson MAJ, Robinson CV. N-glycan microheterogeneity regulates interactions of plasma proteins. *Proc Natl Acad Sci U S A.* 2018;115(35):8763-8.

32. Zhao P, Praissman JL, Grant OC, Cai Y, Xiao T, Rosenbalm KE, et al. Virus-Receptor Interactions of Glycosylated SARS-CoV-2 Spike and Human ACE2 Receptor. *Cell Host Microbe.* 2020;28(4):586-601 e6.

33. Wang D, Baudys J, Bundy JL, Solano M, Keppel T, Barr JR. Comprehensive Analysis of the Glycan Complement of SARS-CoV-2 Spike Proteins Using Signature Ions-Triggered Electron-Transfer/Higher-Energy Collisional Dissociation (ETHcD) Mass Spectrometry. *Anal Chem.* 2020;92(21):14730-9.

34. Shajahan A, Pepi L, Kumar B, Murray N, Azadi P. Site Specific N- and O-glycosylation mapping of the Spike Proteins of SARS-CoV-2 Variants of Concern. *Res Sq.* 2022.
35. Zhu B, Chen Z, Shen J, Xu Y, Lan R, Sun S. Structural- and Site-Specific N-Glycosylation Characterization of COVID-19 Virus Spike with StrucGP. *Anal Chem.* 2022;94(36):12274-9.
36. Campos D, Girgis M, Sanda M. Site-specific glycosylation of SARS-CoV-2: Big challenges in mass spectrometry analysis. *Proteomics.* 2022;22(15-16):e2100322.
37. Newby ML, Fogarty CA, Allen JD, Butler J, Fadda E, Crispin M. Variations within the Glycan Shield of SARS-CoV-2 Impact Viral Spike Dynamics. *J Mol Biol.* 2023;435(4):167928.
38. Krishnan S, Krishnan GP. N-Glycosylation Network Construction and Analysis to Modify Glycans on the Spike (S) Glycoprotein of SARS-CoV-2. *Front Bioinform.* 2021;1:667012.
39. Wang D, Zhou B, Keppel TR, Solano M, Baudys J, Goldstein J, et al. N-glycosylation profiles of the SARS-CoV-2 spike D614G mutant and its ancestral protein characterized by advanced mass spectrometry. *Sci Rep.* 2021;11(1):23561.
40. Saba J, Dutta S, Hemenway E, Viner R. Increasing the productivity of glycopeptides analysis by using higher-energy collision dissociation-accurate mass-product-dependent electron transfer dissociation. *Int J Proteomics.* 2012;2012:560391.
41. Zhang J, Cai Y, Xiao T, Lu J, Peng H, Sterling SM, et al. Structural impact on SARS-CoV-2 spike protein by D614G substitution. *Science.* 2021;372(6541):525-30.
42. Masson GR, Burke JE, Ahn NG, Anand GS, Borchers C, Brier S, et al. Recommendations for performing, interpreting and reporting hydrogen deuterium exchange mass spectrometry (HDX-MS) experiments. *Nat Methods.* 2019;16(7):595-602.
43. Li M, Zhu W, Zheng H, Zhang J. Efficient HCD-pd-EThcD approach for N-glycan mapping of therapeutic antibodies at intact glycopeptide level. *Anal Chim Acta.* 2022;1189:339232.
44. Shen Y, Xiao K, Tian Z. Site- and structure-specific characterization of the human urinary N-glycoproteome with site-determining and structure-diagnostic product ions. *Rapid Commun Mass Spectrom.* 2021;35(1):e8952.
45. Sanda M, Benicky J, Goldman R. Low Collision Energy Fragmentation in Structure-Specific Glycoproteomics Analysis. *Anal Chem.* 2020;92(12):8262-7.
46. Gong Y, Qin S, Dai L, Tian Z. The glycosylation in SARS-CoV-2 and its receptor ACE2. *Signal Transduct Target Ther.* 2021;6(1):396.
47. Miyagi M, Nakazawa T. Determination of pKa values of individual histidine residues in proteins using mass spectrometry. *Anal Chem.* 2008;80(17):6481-7.
48. Tran DT, Banerjee S, Alayash AI, Crumbliss AL, Fitzgerald MC. Slow histidine H/D exchange protocol for thermodynamic analysis of protein folding and stability using mass spectrometry. *Anal Chem.* 2012;84(3):1653-60.
49. Guttman M, Scian M, Lee KK. Tracking hydrogen/deuterium exchange at glycan sites in glycoproteins by mass spectrometry. *Anal Chem.* 2011;83(19):7492-9.
50. Hatvany JB, Gallagher ES. Hydrogen/deuterium exchange for the analysis of carbohydrates. *Carbohydrate research.* 2023;530:108859.
51. Rand KD, Zehl M, Jorgensen TJ. Measuring the hydrogen/deuterium exchange of proteins at high spatial resolution by mass spectrometry: overcoming gas-phase hydrogen/deuterium scrambling. *Acc Chem Res.* 2014;47(10):3018-27.

52. Wollenberg DTW, Pengelley S, Mouritsen JC, Suckau D, Jorgensen CI, Jorgensen TJD. Avoiding H/D Scrambling with Minimal Ion Transmission Loss for HDX-MS/MS-ETD Analysis on a High-Resolution Q-TOF Mass Spectrometer. *Anal Chem.* 2020;92(11):7453-61.
53. Zehl M, Rand KD, Jensen ON, Jorgensen TJ. Electron transfer dissociation facilitates the measurement of deuterium incorporation into selectively labeled peptides with single residue resolution. *J Am Chem Soc.* 2008;130(51):17453-9.
54. Mistarz UH, Bellina B, Jensen PF, Brown JM, Barran PE, Rand KD. UV Photodissociation Mass Spectrometry Accurately Localize Sites of Backbone Deuteration in Peptides. *Anal Chem.* 2018;90(2):1077-80.
55. Woo H, Park SJ, Choi YK, Park T, Tanveer M, Cao Y, et al. Developing a Fully Glycosylated Full-Length SARS-CoV-2 Spike Protein Model in a Viral Membrane. *J Phys Chem B.* 2020;124(33):7128-37.
56. Kumar P, Bhardwaj T, Garg N, Giri R. Microsecond simulations and CD spectroscopy reveals the intrinsically disordered nature of SARS-CoV-2 spike-C-terminal cytoplasmic tail (residues 1242-1273) in isolation. *Virology.* 2022;566:42-55.
57. Li F, Li W, Farzan M, Harrison SC. Structure of SARS coronavirus spike receptor-binding domain complexed with receptor. *Science.* 2005;309(5742):1864-8.
58. Peterle D, DePice D, Wales TE, Engen JR. Increase the flow rate and improve hydrogen deuterium exchange mass spectrometry. *J Chromatogr A.* 2023;1689:463742.
59. Peterle D, Wales TE, Engen JR. Simple and Fast Maximally Deuterated Control (maxD) Preparation for Hydrogen-Deuterium Exchange Mass Spectrometry Experiments. *Anal Chem.* 2022;94(28):10142-50.
60. Bai Y, Milne JS, Mayne L, Englander SW. Primary structure effects on peptide group hydrogen exchange. *Proteins.* 1993;17(1):75-86.
61. Chetty PS, Mayne L, Lund-Katz S, Stranz D, Englander SW, Phillips MC. Helical structure and stability in human apolipoprotein A-I by hydrogen exchange and mass spectrometry. *Proc Natl Acad Sci U S A.* 2009;106(45):19005-10.
62. Gramlich M, Maier S, Kaiser PD, Traenkle B, Wagner TR, Voglmeir J, et al. A Novel PNGase Rc for Improved Protein N-Deglycosylation in Bioanalytics and Hydrogen-Deuterium Exchange Coupled With Mass Spectrometry Epitope Mapping under Challenging Conditions. *Anal Chem.* 2022;94(27):9863-71.
63. Comamala G, Madsen JB, Voglmeir J, Du YM, Jensen PF, Osterlund EC, et al. Deglycosylation by the Acidic Glycosidase PNGase H(+) Enables Analysis of N-Linked Glycoproteins by Hydrogen/Deuterium Exchange Mass Spectrometry. *J Am Soc Mass Spectrom.* 2020;31(11):2305-12.
64. Guo RR, Comamala G, Yang HH, Gramlich M, Du YM, Wang T, et al. Discovery of Highly Active Recombinant PNGase H(+) Variants Through the Rational Exploration of Unstudied Acidobacterial Genomes. *Front Bioeng Biotechnol.* 2020;8:741.
65. Sztain T, Ahn SH, Bogetti AT, Casalino L, Goldsmith JA, Seitz E, et al. A glycan gate controls opening of the SARS-CoV-2 spike protein. *Nat Chem.* 2021;13(10):963-8.
66. Hsu YP, Frank M, Mukherjee D, Shchurik V, Makarov A, Mann BF. Structural remodeling of SARS-CoV-2 spike protein glycans reveals the regulatory roles in receptor-binding affinity. *Glycobiology.* 2023;33(2):126-37.
67. Casalino L, Gaieb Z, Goldsmith JA, Hjorth CK, Dommer AC, Harbison AM, et al. Beyond Shielding: The Roles of Glycans in the SARS-CoV-2 Spike Protein. *ACS Cent Sci.* 2020;6(10):1722-34.

FIGURE LEGENDS

Figure 1 . Representative N-glycan microheterogeneity during HDX-MS at spike sequons N61, N122, N801, N1074, and N1134. The N-terminus (A), central region (B) and C-terminus (C) of spike are shown including HDX peptide coverage (black horizontal lines), N-glycosylation sequons (green horizontal dash within HDX peptide), signal peptide (grey horizontal box), S2' cleavage site (vertical red line), fusion peptide (white horizontal box), and the locations of two disulfide bonds in intact spike (orange brackets marked SS). Specific glycan structures detected at each sequon are cartooned as HexNAc (blue squares), Hexose (green or yellow circles), Fucose (red triangles) and NeuAc (purple diamonds). Glycan structures are illustrative only and were not determined in this study.

Figure 2. Tandem mass spectrum of glycopeptide 597-607 HexNAc(2)Hex(5) including sequon N603. Sample was unlabeled (0 sec D₂O exposure), fragment mass errors are shown in the lower panel. Glycan product ions (green font) from HCD will trigger EThcD MS/MS of a fresh precursor ion packet.

Figure 3. Extracted ion chromatograms (A) and isotopic envelopes (B) of glycopeptide 597-607 HexNAc(2)Hex(5) including sequon N603 (red N). Technical triplicate injections at each D₂O exposure time (central numbers) and both control (black) and heat treatment (blue) conditions were injected in randomized order.

Figure 4. Box and whiskers uptake plots of 12 glycopeptides including sequon N603. The left, center, and right boxes are N = 6, 2, and 4 unique glycopeptides (sequences, glycans, or charge states), respectively. Dashed lines linking boxes indicate the same D₂O exposure time and control or heat denatured state, × indicates mean.

Figure 5. Isotopologue ratios of glycopeptide 597-607 HexNAc(2)Hex(5) fragment ions (see Figure 1 for a typical MS/MS spectrum of this peptide). *Inset* : the ratio of M0 (monoisotopic peak) to M1 (first M + 1 isotopic peak) was measured for HexNAc (204/205) and ¹³C₈ (818/819) in a representative technical replicate at each state and D₂O exposure time. As product ions shifted to a deuterated distribution the ratio decreased. N = 3 to 6 averaged MS/MS scans for each bar, error bars are one standard deviation. At H240 and H960 the ¹³C₈ M0 ion was not detected.

Figure 6: Heat map data (960 sec) overlaid on a model based upon PDBs 6VSB and 6VXX (55), view of central trimer head with stalk at lower left corner. Without heat treatment (A) spike labeled between 0-37% indicated by white to red color. Regions with no coverage are green. Taking the difference between heat treatment and control (B) shows both decreased labeling (magenta color, one example is furin site) and increased labeling (yellow color, trimer core is an example). Regions with no coverage are blue.

Figure S1 . The effect of temperature and limited trypsin digestion on the conformation of SARS-CoV-2 spike protein (Omicron variant, Hexapro, His tag). Lane 1: PageRuler Unstained Protein Ladder, component MWs as indicated; Lane 2: empty; Lane 3: 0.5 µg spike, 25°C 1 hr, trypsin digestion as described in Experimental; Lane 4: 0.5 µg spike, 35°C 1 hr, trypsin digestion as described in Experimental; Lane 5: 0.5 µg spike, 45°C 1 hr, trypsin digestion as described in Experimental; Lane 6: 0.5 µg spike, 55°C 1 hr, trypsin digestion as described in Experimental; Lane 7: 0.5 µg spike, 65°C 1 hr, trypsin digestion as described in Experimental. Gel is a non-reducing 4-12% Bis-Tris run in MES buffer at 100 V for 36 min, bands were visualized with SYPRO Ruby Protein Gel Stain (Life Technologies #S12000).

Figure S2 . Coverage map of 614G HexaPro Spike protein showing 561 peptides including 106 glycopeptides. Green font is protein coverage (84%), green lines under N residues indicate glycosylation detected at that N-glycosylation sequon (9 of 22).

Figure S3 . Distinct glycopeptide deuterium uptake patterns at sequon N61 of SARS-CoV-2 spike protein. Data for all glycopeptides covering N61 (top panel) shows higher uptake for the seven glycopeptides not including sequence HAIH (lower right panel) compared to the four glycopeptides including this sequence (lower left panel) after heat treatment.

Figure S4 . Isotopologue ratios of glycopeptide¹¹³²IVNNTVYDPLQPEL¹¹⁴⁵HexNAc(4)Hex(3)Fuc(1) product ions. The ratio of isotopologue M0 to isotopologue M1 was measured for HexNAc (204/205), $\tilde{y}3$ (358/359) and $\tilde{y}6$ (696/697) in 2 or 3 technical replicates at each state and exposure time. As fragment ions shift to a deuterated distribution the ratio decreases. N = 3 to 6 averaged MS/MS scans for each bar.

Figure 2, top

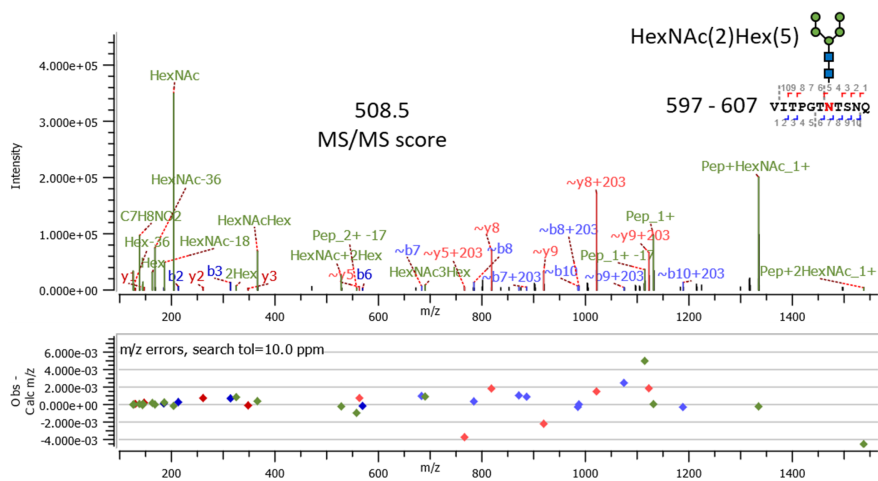


Figure 3, top

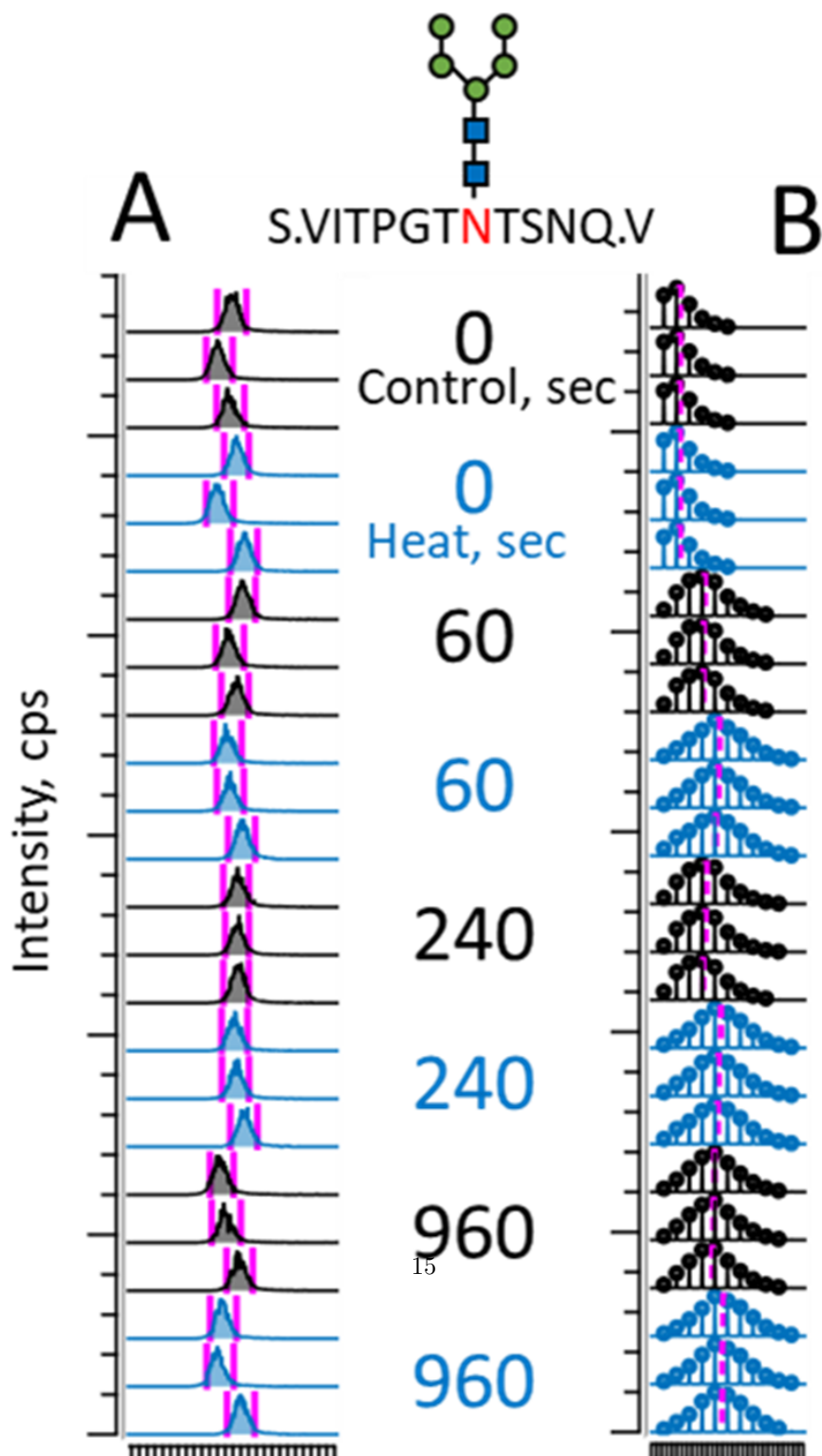


Figure 4, top

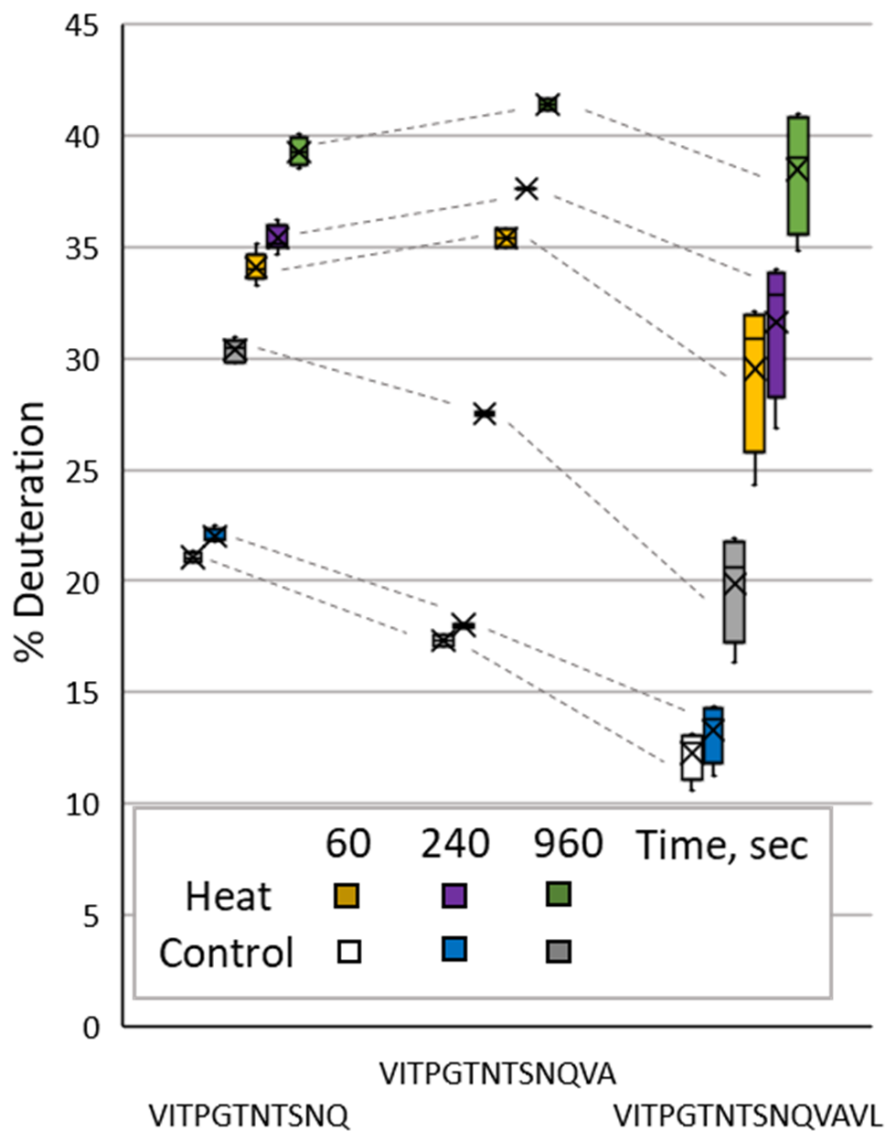


Figure 6, top

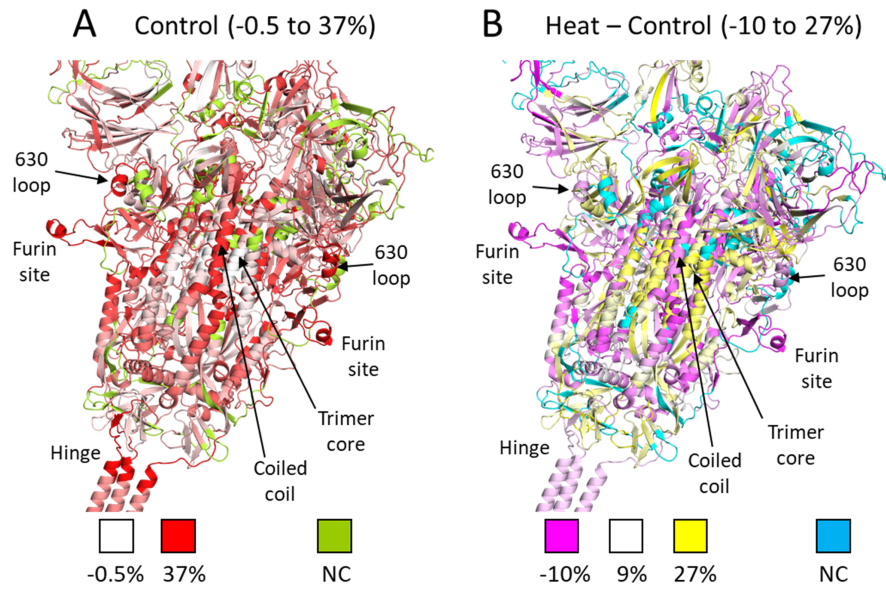


Figure S1, top

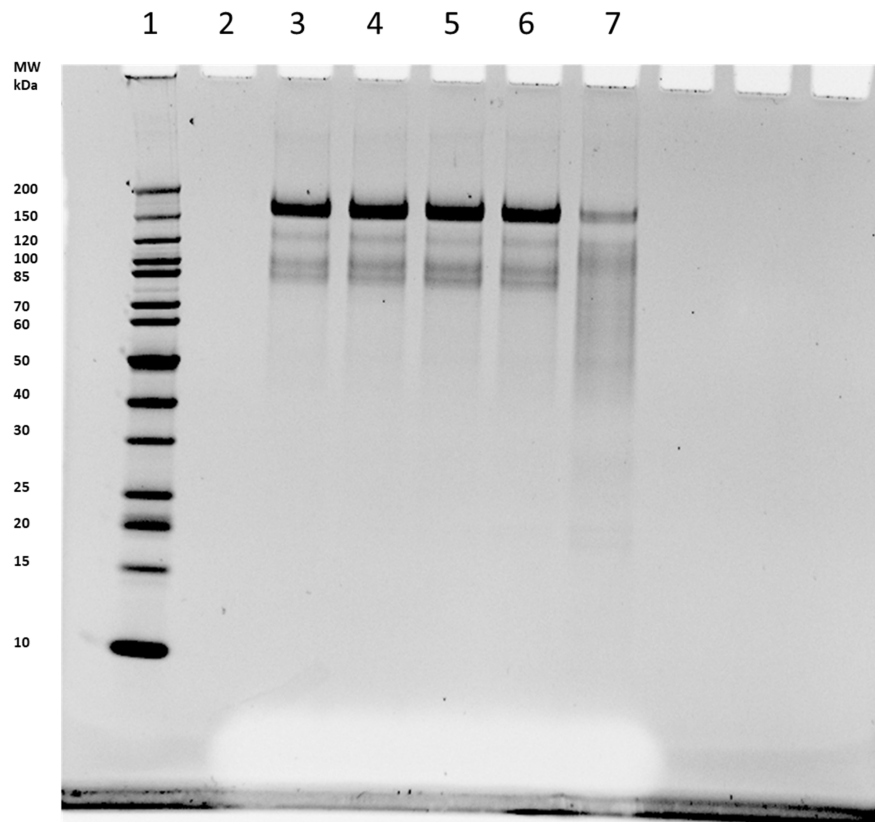


Figure S2, top

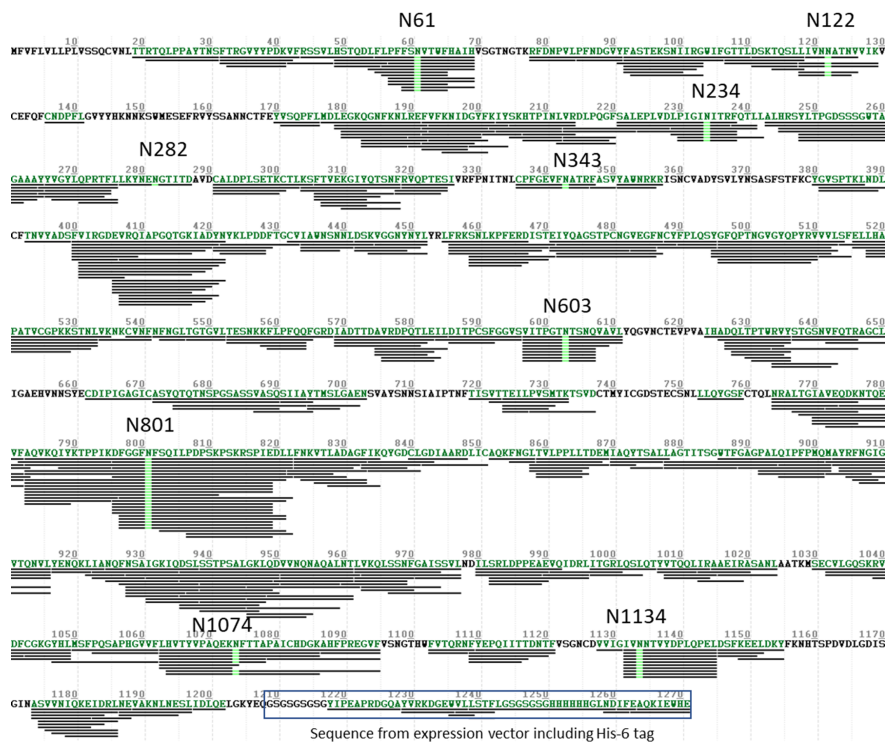


Figure S3, top

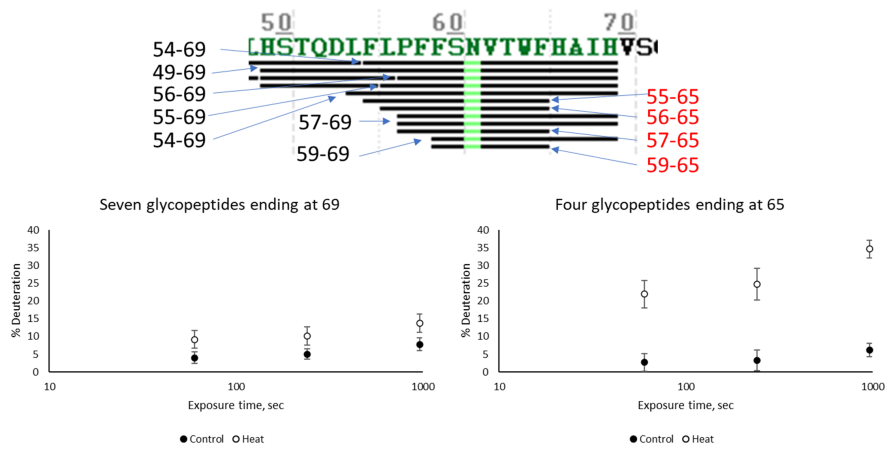


Figure S4, top

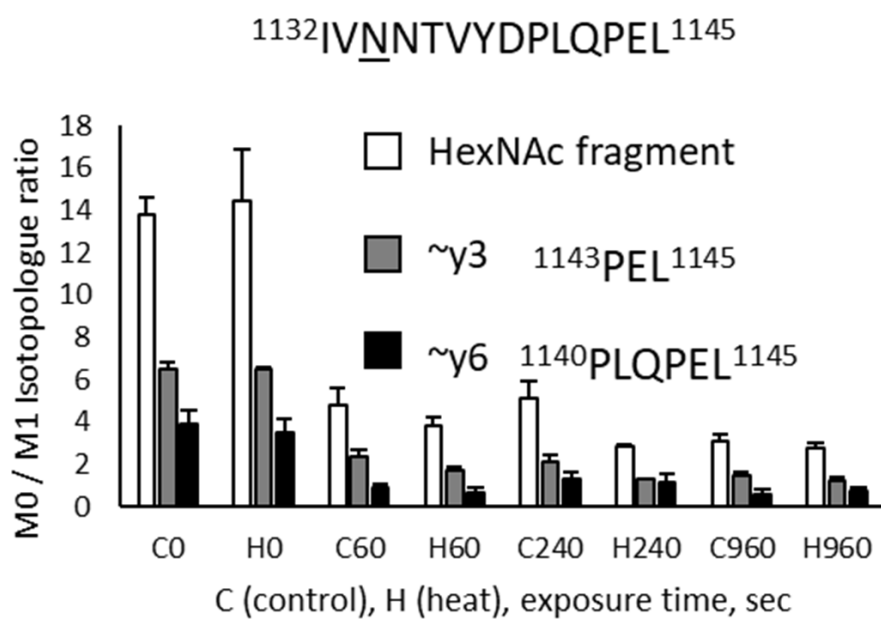


Figure 1, top

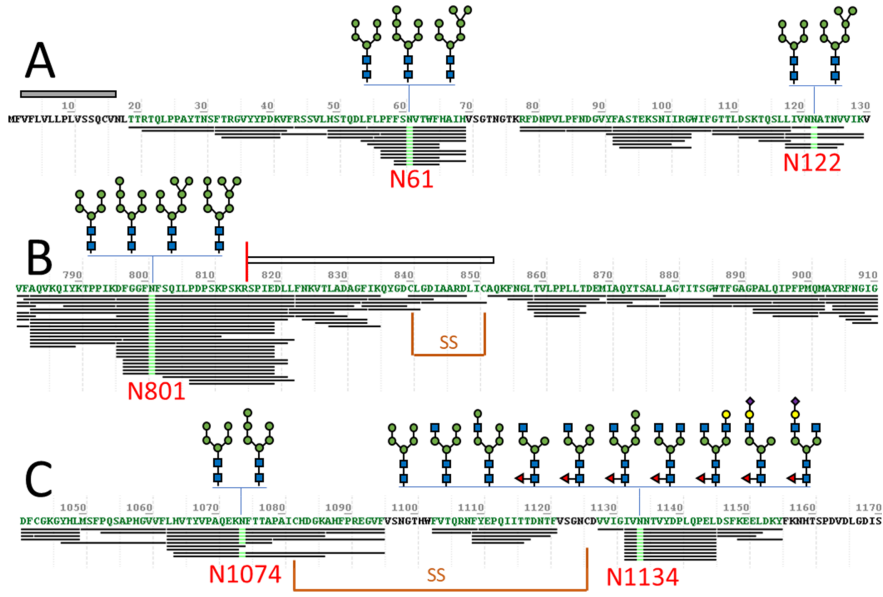
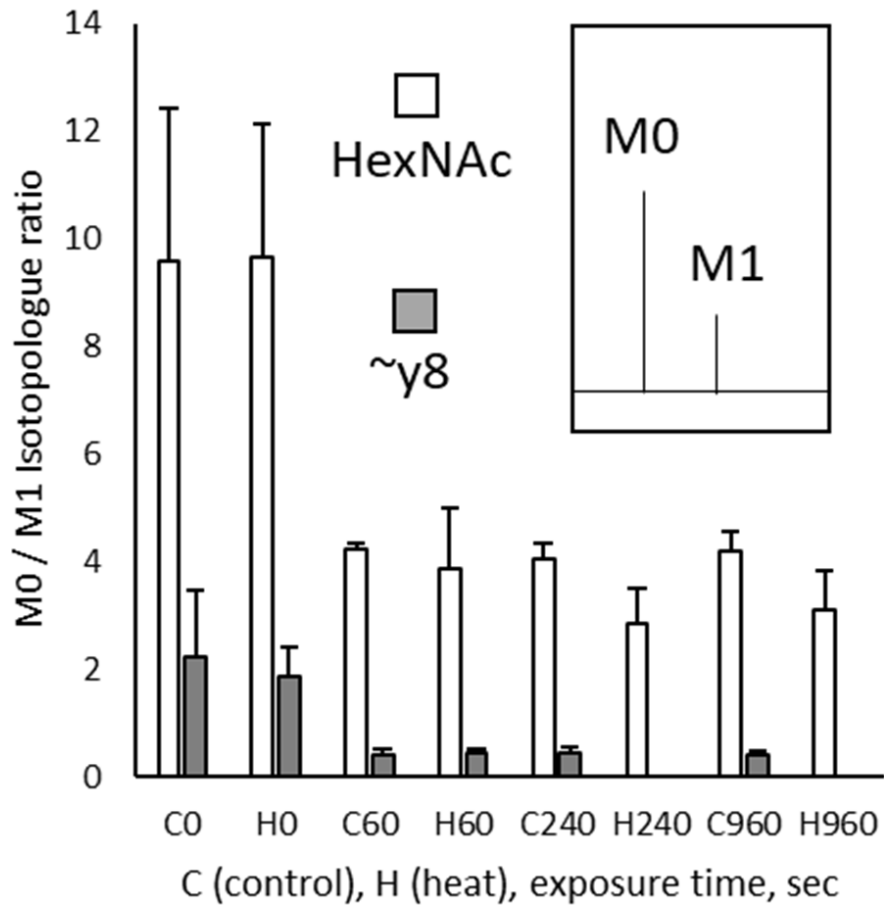


Figure 5, top



Hosted file

Supplementary Table 2.xlsx available at <https://authorea.com/users/665162/articles/666552-inclusion-of-deuterated-glycopeptides-provides-increased-sequence-coverage-in-hydrogen-deuterium-exchange-mass-spectrometry-analysis-of-sars-cov-2-spike-glycoprotein>

Hosted file

Supplementary Table 3.csv available at <https://authorea.com/users/665162/articles/666552-inclusion-of-deuterated-glycopeptides-provides-increased-sequence-coverage-in-hydrogen-deuterium-exchange-mass-spectrometry-analysis-of-sars-cov-2-spike-glycoprotein>

Hosted file

Supplementary Table I - Inclusion of Glycopeptides.docx available at <https://authorea.com/users/665162/articles/666552-inclusion-of-deuterated-glycopeptides-provides-increased-sequence-coverage-in-hydrogen-deuterium-exchange-mass-spectrometry-analysis-of-sars-cov-2-spike-glycoprotein>